JPE 15-5-24

http://dx.doi.org/10.6113/JPE.2015.15.5.1380
ISSN(Print): 1598-2092 / ISSN(Online): 2093-4718

# Loss Analysis and Comparison of High Power Semiconductor Devices in 5MW PMSG MV Wind Turbine Systems

Kihyun Lee*, Yongsug Suh†, and Yongcheol Kang*

*,†Department of Electrical Engineering, Chonbuk National University, Jeonju, Korea

**Abstract**

This paper provides a loss analysis and comparison of high power semiconductor devices in 5MW Permanent Magnet Synchronous Generator (PMSG) Medium Voltage (MV) Wind Turbine Systems (WTSs). High power semiconductor devices of the press-pack type IGCT, module type IGBT, press-pack type IGBT, and press-pack type IEGT of both 4.5kV and 6.5kV are considered in this paper. Benchmarking is performed based on the back-to-back type 3-level Neutral Point Clamped Voltage Source Converters (3L-NPC VSCs) supplied from a grid voltage of 4160V. The feasible number of semiconductor devices in parallel is designed through a loss analysis considering both the conduction and switching losses under the operating conditions of 5MW PMSG wind turbines, particularly for application in offshore wind farms. This paper investigates the loss analysis and thermal performance of 5MW 3L-NPC wind power inverters under the operating conditions of various power factors. The loss analysis and thermal analysis are confirmed through PLECS Blockset simulations with Matlab Simulink. The comparison results show that the press-pack type IGCT has the highest efficiency including the snubber loss factor.

**Key words:** Junction Temperature, Medium Voltage, Multi-level Converter, Power Semiconductor Devices, Voltage Source Converters, Wind Turbine Systems

## I. INTRODUCTION

In the multi-MW wind turbine market, the maximum power rating of commercial wind turbines has been increased to more than 5MW with the aim of generating more power from wind power sites [1]. The power electronic converters in medium-voltage level applications are generally realized as multi-level (ML) VSCs instead of 2L-VSCs in order to improve the performance factors in terms of switch power losses, harmonic distortion, and common mode voltage/current [2], [3]. In the family of multi-level (ML) inverters, the three-level topology, called the Neutral Point Clamped (NPC) inverter, is one of the few topologies that have received a reasonable consensus in the high power community. These NPC inverters have also been implemented successfully in industrial applications for high power drives and wind turbines [2]-[4].

Manuscript received Nov. 6, 2014; accepted May 4, 2015
Recommended for publication by Associate Editor Trillion Q Zheng.
†Corresponding Author: ysuh@jbnu.ac.kr
Tel: +82-63-270-3381, Fax: +82-63-270-2461, Chonbuk Nat'l University
*Dept. of Electrical Eng., Chonbuk Nat'l University, Korea

In multi-MW wind turbine systems, there are many different types of power converter topologies and high-power switching devices in use. In particular, the recent development of high power semiconductor technology has resulted in a wide variety of practical power devices. The benchmarking of these topologies and their optimal power switches is important for industry to select the most feasible solution in the product development of wind turbines. In general, a comparison of various power switches involves a great deal of engineering work considering many different aspects of device characteristics. Therefore, it is necessary to pick critical performance factors on which the comparison for devices is made so that the selection of the most feasible power device can be made with meaningful engineering work and insight.

This paper investigates the utilization of the four most feasible high power switching devices for 5MW PMSG WTSs; the press-pack type IGCT, module type IGBT, press-pack type IGBT, and press-pack type IEGT. The power converter topology of 3L-NPC VSCs is selected as the main platform for the device comparison. Power loss dissipated in the semiconductor devices is one of the most important

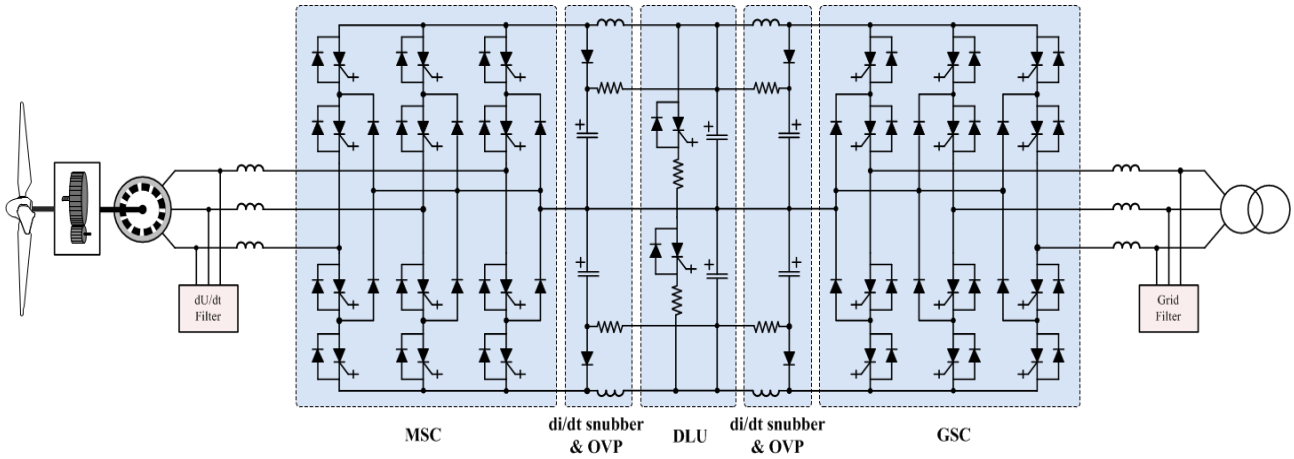


Fig. 1. Back-to-back type 3L-NPC VSCs for 5MW PMSG MV wind turbines.

performance factors in high power drives considering the total system efficiency and the requirements in terms of the cooling system. In addition, a power loss analysis gives an engineer insight into cost-effective system designs [5], [6]. This paper compares four different high power switching devices with respect to power loss dissipation. Furthermore, this paper investigates a transient thermal description of the IGCT platform in 3L-NPC VSCs. 6.5kV and 4.5kV class devices are considered in the loss calculation of the 3L-NPC VSCs. The loss distribution among several switching devices in the converter including the snubber circuit is also explained in this paper.

This paper is structured in four main sections. Section II describes the power semiconductor devices under comparison for a 5MW PMSG WTS. Section III discusses the electro-thermal modeling of the power semiconductor devices. Section IV presents simulation results of 3L-NPC VSCs in a 5MW PMSG MV WTS. Finally, a comparison of the losses in 3L-NPC VSCs is shown in Section V.

## II. Power Semiconductor Devices under Comparison

A simplified schematic of the back-to-back type 3L-NPC VSCs for 5MW PMSG MV wind turbines with the generator connected to a grid is presented in Fig. 1 [2]-[7]. The semiconductor devices commonly used in high power converters are IGBTs (in a module or press-pack package), press-pack type IEGTs and IGCTs for 3L-NPC converters. The recent technological development of 4.5 kV and 6.5 kV IGCTs, IGBTs, and IEGTs has been enabling a substantial improvement of MV converters in many aspects [8], [9]. These four major types of semiconductor devices are considered in this paper. The major operating characteristics of the target semiconductor devices are summarized in Table I and are used in the loss analysis throughout this paper. The important characteristics for the loss calculation are the threshold voltage ($V_{TO}$), slope resistance ($R_T$) as a function of the collector/anode current, turn-on energy ($E_{on}$), turn-off energy ($E_{off}$), diode reverse recovery energy ($E_{rr}$), maximum operating junction temperature ($T_{vj\_max}$), and thermal resistance ($R_{th}$).

### *A. Press-Pack Type IGCT for MV Converters*

MV IGCT press-pack devices are mainly used in high power industrial applications owing to their advantageous features such as press-pack housing cases, a higher thermal/power cycling capability, and explosion-free failure mode [5]. Recently, a 10kV IGCT device has been introduced and its switching capability has been confirmed [10]. In this paper, a 6.5kV/3800A press-pack type IGCT (ABB 5SHY42L6500) is considered for the loss analysis [11]. As for the anti-parallel and neutral point clamped diode, a 6.0kV/1100A press-pack type FRD (ABB 5SDF10H6004) is employed [12].

### *B. Module Type IGBT for MV Converters*

Module type IGBTs are widely accepted in the market for the power range below 3-4 MW approximately. MV IGBTs having a blocking voltage of 6.5kV have been developed by several manufacturers and employed in many industrial applications. The continuous switching current capability of 6.5kV IGBT modules has reached around 750A. In this paper, a 6.5kV/750A module type IGBT (ABB 5SNA0750G650300) is considered for the loss analysis [13].

### *C. Press-Pack Type IGBT for MV Converters*

The recently developed press-pack type IGBT devices combine the advantages of IGBTs with those of press-pack cases. Thus, press-pack IGBTs have become a competitor for IGCTs in medium and high power industrial applications such as the MV drives for wind turbines [14]. In this paper, a 4.5kV/2400A press-pack type IGBT (Westcode, IXYS T2400GB45E) is considered for the loss analysis [15].

### *D. Press-Pack Type IEGT for MV Converters*

As a high-voltage and large-capacity power semiconductor device to replace conventional GTO thyristors, the Injection Enhanced Gate Transistor (IEGT) has been developed in recent

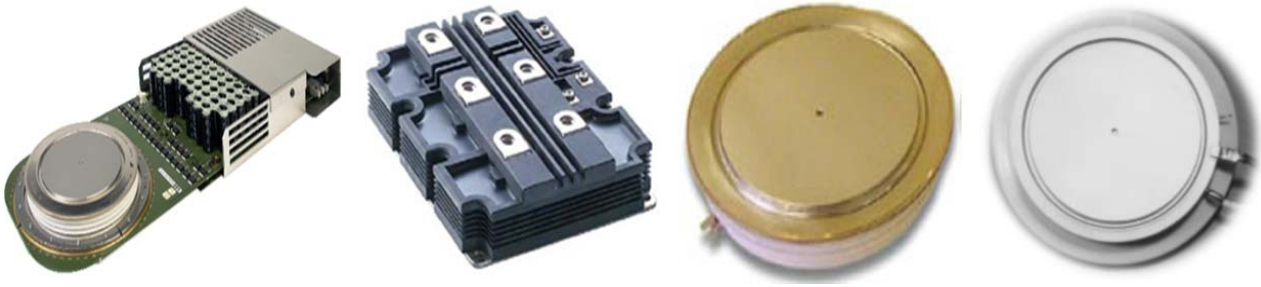

Press-pack type IGCT | Module type IGBT | Press-pack type IGBT | Press-pack type IEGT

Fig. 2. Target power semiconductor devices for MV wind turbines [11], [13], [15], [18].

TABLE I
CIRCUIT PARAMETERS AND OPERATING CONDITIONS [11], [12], [13], [15], [18]

| Device | IGCT | Module type IGBT | | Press-pack IGBT | Press-pack IEGT | Press-pack Diode |
|---|---|---|---|---|---|---|
| Manufacturer | ABB | ABB | | Westcode, IXYS | Toshiba | ABB |
| Code | 5SHY 42L6500 | 5SNA 0750G650300 | | T2400GB45E | ST2100GXH22A | 5SDF 10H6004 |
| Blocking Voltage | 6.5 kV | 6.5 kV | | 4.5 kV | 4.5 kV | 6.0 kV |
| $I_{TGQM}$ | 3800A | - | | - | - | - |
| $I_{C,nom}$ / $I_{CM}$ | - | 750A / 1500A | | 2400A / 4800A | 2100A / 5500A | - |
| $I_{F(AV)M}$ | - | - | | - | - | 1100A |
| Part | GCT-part | IGBT-part | Diode-part | IGBT-part | - | Diode-part |
| $V_{TO}$ (Max.) | 1.88 V | 2.0 V | 2.5 V | 1.49 V | 3.0 V | 1.5 V |
| $R_T$ (Max.) | 0.56 mΩ | 2.5 mΩ | 1.3 mΩ | 1.05 mΩ | 1.0 mΩ | 0.6 mΩ |
| $E_{on}$ (Max.) | 3.1 J | 6.4 J | - | 15 J | 18.4 J | - |
| $E_{off}$ / $E_{rr}$ (Max.) | 44 J | 5.3 J | 2.7 J | 14 J | 17 J | 5 J |
| Meas. condition | 4kV / 3800A | 3.6kV / 750A | | 2.8kV / 2400A | 3.0kV / 2100A | 2.9kV / 1000A |
| $T_{vj\_max.}$ | 125℃ | 125℃ | | 125℃ | 125℃ | 125℃ |
| $R_{th(j-c)}$ | 8.5 K/kW | 11 K/kW | 21 K/kW | 5.2 K/kW | 5.25 K/kW | 12 K/kW |
| $R_{th(c-h)}$ | 3 K/kW | 9 K/kW | 18 K/kW | 3 K/kW | 3 K/kW | 3 K/kW |
| $R_{th(h-a)}$ | 6 K/kW | 10 K/kW | 10 K/kW | 6 K/kW | 6 K/kW | 6 K/kW |

years and applied in a practical use. This development was led by Toshiba and GE Companies. High-voltage, large-capacity, and full-controlled power device of the IEGT type are intended to combine the advantages of IGBT devices and GTO devices. The press-pack type 4.5kV IEGTs have been placed on the market, mainly for the use in medium voltage converters [16], [17]. In this paper, a 4.5kV/2100A press-pack IEGT (Toshiba ST2100GXH22A) is considered for the loss analysis [18].

## III. ELECTRO-THERMAL MODELING OF THE POWER SEMICONDUCTOR DEVICES

### A. Power Loss Modeling of Semiconductors Devices

The losses of power semiconductor device are approximated by analytical expressions in terms of voltage and current.

Fig. 3 shows a simplified loss estimation model for power semiconductor devices.

*1) Conduction Losses:* The total semiconductor device loss

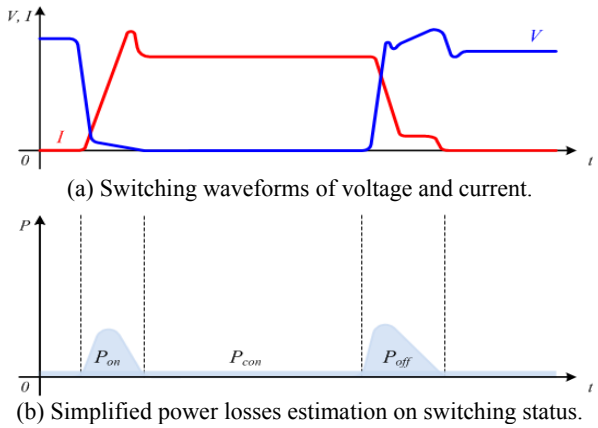


(a) Switching waveforms of voltage and current.

(b) Simplified power losses estimation on switching status.

Fig. 3. Simplified device switching waveforms and its power losses.

$P_t$ consists of the conduction loss $P_{cond}$ and the switching loss $P_{switching}$ [19] [20];

$$P_t = P_{cond} + P_{switching} = P_{cond} + P_{on} + P_{off} \quad (1)$$

The conduction loss of each power semiconductor depends on the instantaneous on-state voltage $v_{sw}(t)$ and the instantaneous switching current $i(t)$ passing through it. The forward on-state voltage of the power semiconductor device, $v_{sw}(t)$ can be modeled by using a first-order linear approximation comprised of a threshold voltage $v_{on}$ and a series resistance $R_{on}$ as follows;

$$v_{sw}(t) = v_{on} + R_{on} \cdot i(t) \quad (2)$$

The total conduction loss in the power semiconductors can be expressed as;

$$\begin{aligned} P_{cond} &= \frac{1}{T}\int v_{sw}(t)\cdot i(t)dt \\ &= \frac{1}{T}\int \{v_{on} + R_{on}\cdot i(t)\} i(t)dt \\ &= v_{on} I_{avg} + R_{on}(I_{rms})^2 \end{aligned} \quad (3)$$

where $T$ is the fundamental period of the converter [21].

*2) Switching Losses:* The switching loss of the power semiconductor device is determined by the total commutation time in which the device is turned on/off, and by the voltage *v(t)* and current *i(t)* across the device. The energy dissipated during commutations is made up of $E_{on}$, $E_{off}$, and $E_{rr}$, for the turn-on, turn-off, and diode reverse recovery, respectively. This information is provided by the device manufacturer on their datasheet. The average switching power loss $P_{switching}$ over a complete fundamental period $T$ may be determined by summing all of the commutations of a device during a respective interval of time. The switching loss for the turn-on, turn-off, and diode revers recovery can be expressed as;

$$\begin{aligned} P_{on} &= E_{on} \times f_{sw} \\ &= \frac{V_{on(measure)}}{V_{test}} \times \frac{I_{on(measure)}}{I_{test}} \times E_{on(spec)} \times f_{sw} \end{aligned} \quad (4)$$

$$\begin{aligned} P_{off} &= E_{off} \times f_{sw} \\ &= \frac{V_{off(measure)}}{V_{test}} \times \frac{I_{off(measure)}}{I_{test}} \times E_{off(spec)} \times f_{sw} \end{aligned} \quad (5)$$

$$\begin{aligned} P_{off} &= E_{rr} \times f_{sw} \\ &= \frac{V_{off(measure)}}{V_{test}} \times \frac{I_{off(measure)}}{I_{test}} \times E_{rr(spec)} \times f_{sw} \end{aligned} \quad (6)$$

Equation (4), (5), and (6) represent linear approximations of the actual switching loss for the turn-on, turn-off, and diode reverse recovery based on the specific values ($E_{on(spec)}$, $E_{off(spec)}$, and $E_{rr(spec)}$) provided by the manufacturer. Although the switching loss can vary depending on the gate impedance, parasitic circuit elements, and snubber characteristics, this linear approximation gives fairly good accuracy particularly in the vicinity of the manufacturer's test point ($V_{test}$ and $I_{test}$) and snubber condition [5].

In some cases, the turn off loss of an IGBT device, unlike IGCT devices, is not linear. Therefore, the switching loss of an IGBT can be modeled as a 2nd-order polynomial curve having a parabolic shape like the following.

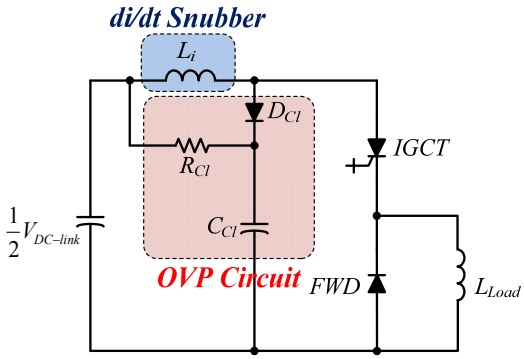


Fig. 4. OVP clamp and *di/dt* snubber circuit of IGCT in the upper-half part of 3L-NPC VSC.

$$E_{switching} = f(i) = k_0 + k_1 i + k_2 i^2 \quad (7)$$

where $k_0$, $k_1$, and $k_2$ are polynomial coefficients. However, even in the case of (7), the approximations of $P_{on}$ and $P_{off}$, by (4)-(6), have a quite high engineering accuracy.

### *B. Loss Modeling of a Snubber Circuit for the IGCT Platform*

Converters employing IGCTs need a *di/dt* limiting inductance to meet the required *di/dt* characteristics during switching on transients. This *di/dt* limiting inductor ($L_i$) usually necessitates an additional over voltage protection snubber or clamping circuitry, as shown in Fig. 1. This snubber circuitry dissipates additional power loss and gives a rise to an important loss factor which should be taken into consideration for a comprehensive loss comparison.

Fig. 4 presents an equivalent circuit of the *di/dt* limiting inductor, over voltage protection, and the particular IGCT being subject to switching transients in Fig. 1. At the instant of switching off, the stored magnetic energy in the *di/dt* limiting inductor due to the on-state current of the IGCT is given by;

$$E_{L_i} = \frac{1}{2} L_i \cdot i(t)^2 \quad (8)$$

This stored energy is mainly dissipated in the snubber resistor ($R_{Cl}$) or fed back to charge the dc link capacitor ($C_{DC\text{-}link}$) [22]. In this paper, the total stored energy in the di/dt limiting inductor is considered to be snubber circuit power loss since the loss analysis is performed to compare the full functionality of different power semiconductor switching devices on an equal basis. Therefore, the clamp (snubber) circuit loss $P_{cl}$ can be expressed as;

$$P_{cl} = \left(\sum_{k=1}^{n} E_{L_i}\right) \times f_{sw} = \left\{\frac{1}{2} L_i \sum_{k=1}^{n} i_k(t)^2\right\} \times f_{sw} \quad (9)$$

### *C. Thermal Modeling of the Semiconductor Devices*

The thermal performance of the power semiconductor devices is closely related to the reliability and cost of the whole

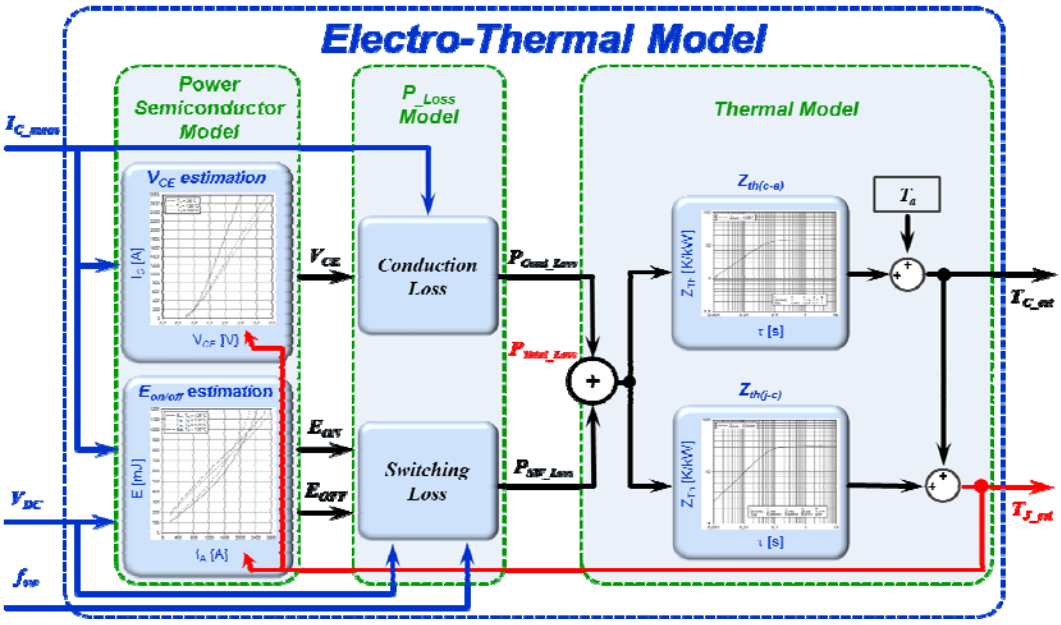


Fig. 5. Electro-thermal model structure for junction temperature of power semiconductor [25].

power converter system [23]. The power loss modeling can be implemented based on the current and voltage values in the power devices. Afterwards, the thermal modeling is applied to the estimation of the loss dissipation. The electro-thermal model deals with the analysis of both the electrical and thermal performances, which interact with each other by the power dissipation of the electronics devices [24]. The main purpose of the electro-thermal model is to estimate the junction and case temperature for the 3L-NPC VSCs. The electro-thermal model is implemented for a press-pack type IGCT (5SHY42L6500) and Diode (5SDF10H6004) from ABB.

Fig. 5 shows the electro-thermal models involved in the model of the power device, power loss, and thermal model [25]. According to Fig. 5, the junction temperature is determined by the power losses of the power semiconductors. The steady state average junction temperature of each power semiconductor device can be expressed as follows according to [26]. $T_j$ and $P_t$ represent the junction temperature and the total semiconductor device loss, respectively [24]. The junction temperature is obtained as;

$$T_j[^\circ C] = \left(P_t[W] \times R_{th}[^\circ C/W]\right) + T_a[^\circ C] \quad (10)$$

The total thermal resistance $R_{th}$ consists of $R_{th(j-c)}$, $R_{th(c-h)}$, and $R_{th(h-a)}$;

$$R_{th} = R_{th(j-c)} + R_{th(c-h)} + R_{th(h-a)} \quad (11)$$

$R_{th(j-c)}$ is the thermal resistance from the junction-to-case, $R_{th(c-h)}$ is the thermal resistance from the case-to-heatsink, $R_{th(h-a)}$ is the thermal resistance from the heatsink-to-ambient.

In order to obtain the transient behavior of the junction temperature, the transient thermal impedance should be taken into consideration in the thermal modeling of the semiconductor devices. The transient thermal impedance is

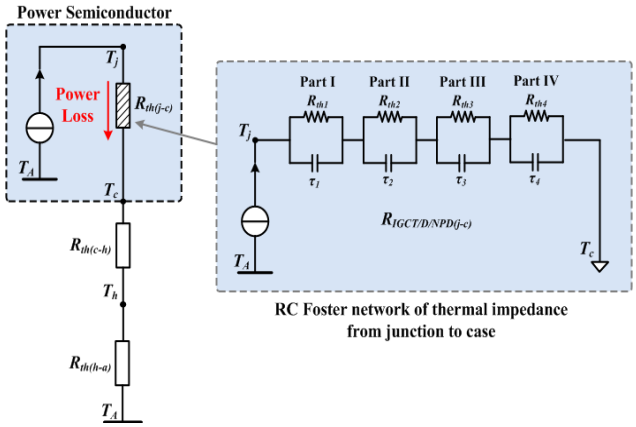


Fig. 6. Thermal model of power semiconductor devices with four-layer Foster RC network.

defined to be the transient response of the junction temperature against the unit step power loss. Therefore, the transient thermal impedance indirectly provides the information on the thermal resistance and capacitance of the Foster RC network model.

The curve for the transient thermal impedance $Z_{th(j-c)}$ can be fit into the series of the exponential term as (12).

$$Z_{th(j-c)}(t) = \sum_{i=1}^{n} R_{th(j-c),i}\left(1 - e^{-t/\tau_i}\right) \quad (12)$$

The thermal impedance from the junction to the case $Z_{th(j-c)}$ is modeled as a four-layer Foster RC network as depicted in Fig. 6. The case to the heatsink thermal impedance is modeled as a simple thermal resistor. Furthermore, the ambient temperature is set to 30℃. It is worth mentioning that a number of the four parameters are more than sufficient for a good estimation of the

TABLE II
PARAMETERS OF THE THERMAL IMPEDANCE FOR A IGCT PLATFORM

| Thermal Impedance | $R_{th(j-c)}$ | | | | $R_{th(c-h)}$ |
|---|---|---|---|---|---|
| | Part I | Part II | Part III | Part IV | |
| $R_{iIGCT}$(K/kW) | 5.562 | 1.527 | 0.868 | 0.545 | 3 |
| $\tau_{iIGCT}$(s) | 0.5119 | 0.0896 | 0.0091 | 0.0024 | - |
| $R_{iDiode}$(K/kW) | 7.440 | 2.000 | 1.840 | 0.710 | 3 |
| $\tau_{iDiode}$(ms) | 0. 4700 | 0.0910 | 0.0100 | 0.0047 | - |
| $R_{iNPD}$(K/kW) | 7.440 | 2.000 | 1.840 | 0.710 | 3 |
| $\tau_{iNPD}$(ms) | 0. 4700 | 0.0910 | 0.0100 | 0.0047 | - |

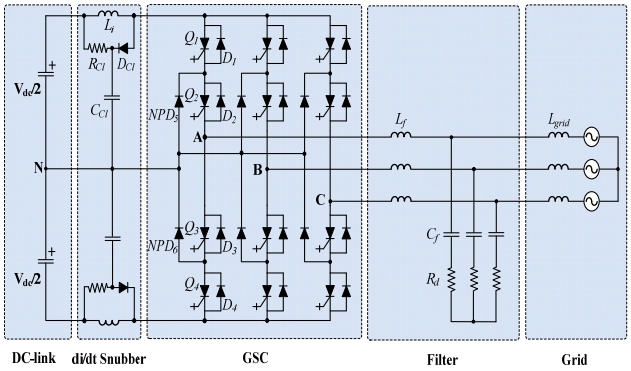


Fig. 7. 3L-NPC VSCs for loss analysis in 5MW PMSG MV WTS.

Foster Network. The parameters for a press-pack type 6.5kV IGCT platform are summarized in Table II [11], [12], [27].

## IV. SIMULATION RESULTS OF THE 3L-NPC VSCS IN A 5MW PMSG MV WTS

### A. Medium-Voltage 3L-NPC VSCs Topology

Fig. 7 shows the 3L-NPC VSCs topology for the loss analysis of selected high power semiconductors in a 5MW PMSG MV WTS. Each leg of the VSC consists of two neutral-point clamped diodes, four switches, and four anti-parallel diodes. The DC-bus voltage is split into three-levels by two series connected capacitors. The middle point of the two capacitors N can be defined as a neutral point. The output voltage $v_{AN}$ has three states ($V_{dc}$/2, 0, and $-V_{dc}$/2) in each leg, which are produced by specific conduction paths depending on the output current direction and the output voltage polarity. Due to the relatively low switching frequency, a 2nd-order LC-filter system has been employed at the grid side of the converter to meet the harmonic constraints of the grid code, for example IEEE-519 [28]. In addition, a *di/dt* snubber is essential for all of the IGCT converters to achieve the required *di/dt* characteristics during switching on and to mitigate the reverse recovery stress on the fast diodes.

### B. Power Loss Distribution in a 5MW PMSG WTS

The simulation is performed based on the parameters of a 5MW MV 3L-NPC VSC as specified in Table III. Since the Grid Side Converter (GSC) is a 3L-NPC type converter connected to an ac line of 4160V, the nominal dc-link voltage is chosen to be 7kV. The switching frequency, i.e. the PWM carrier frequency, adopted for the GSC is set to 1020Hz. This switching frequency is selected to be 17 times the fundamental frequency. The selection of the switching frequency is done on the basis of compromising the switching loss and the harmonic content of the ac input current.

TABLE III
SIMULATION PARAMETERS OF 5MW MV 3L-NPC VSCS

| Parameter | Symbol | Value | Per unit |
|---|---|---|---|
| Output Power | $P_{rated\text{-}out}$ | 5 MW | 1.0 |
| Frequency | $f_{grid}$ | 60 Hz | 1.0 |
| Grid side inductance | $L_{grid}$ | 1.56 mH | 0.17 |
| Grid side input voltage | $V_{LL}$ | 4.16 kV | 1.0 |
| Grid side input current | $I_{AC\_input}$ | 708 A | 1.0 |
| Switching frequency | $f_{GSC\_PWM}$ | 1020 Hz | - |
| DC-link voltage | $V_{DC\text{-}link}$ | 7 kV | - |
| DC-link capacitance | $C_{DC\text{-}link}$ | 2.6 mF | - |
| AC filter inductance | $L_f$ | 1.5 mH | 0.16 |
| AC filter capacitance | $C_f$ | 0.35 mF | 0.45 |

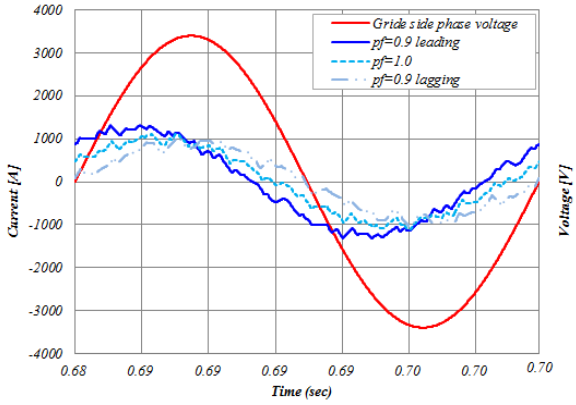


Fig. 8. Waveforms of ac input current at the converter pole under inverter operating mode (Positive current flowing into converter from grid).

In Fig. 8, the ac input currents at the converter pole under the three different power factor conditions (0.9 leading condition, 1.0, and 0.9 lagging condition) are given with respect to the grid phase voltage. It is noted that the amplitude of the ac input current for the case of the 0.9 leading condition under inverter operating mode is at its largest among three conditions. This is due to the fact that the grid side LC-filter adds an additional leading power factor so that the input current at the converter pole requires an increased leading angle to generate the 0.9 leading power factor at the ac input, i.e. upstream of the grid side LC-filter.

Figs. 9 and 10 show waveforms of the switching current and voltage for the 6.5kV IGCTs in each phase-leg during one ac

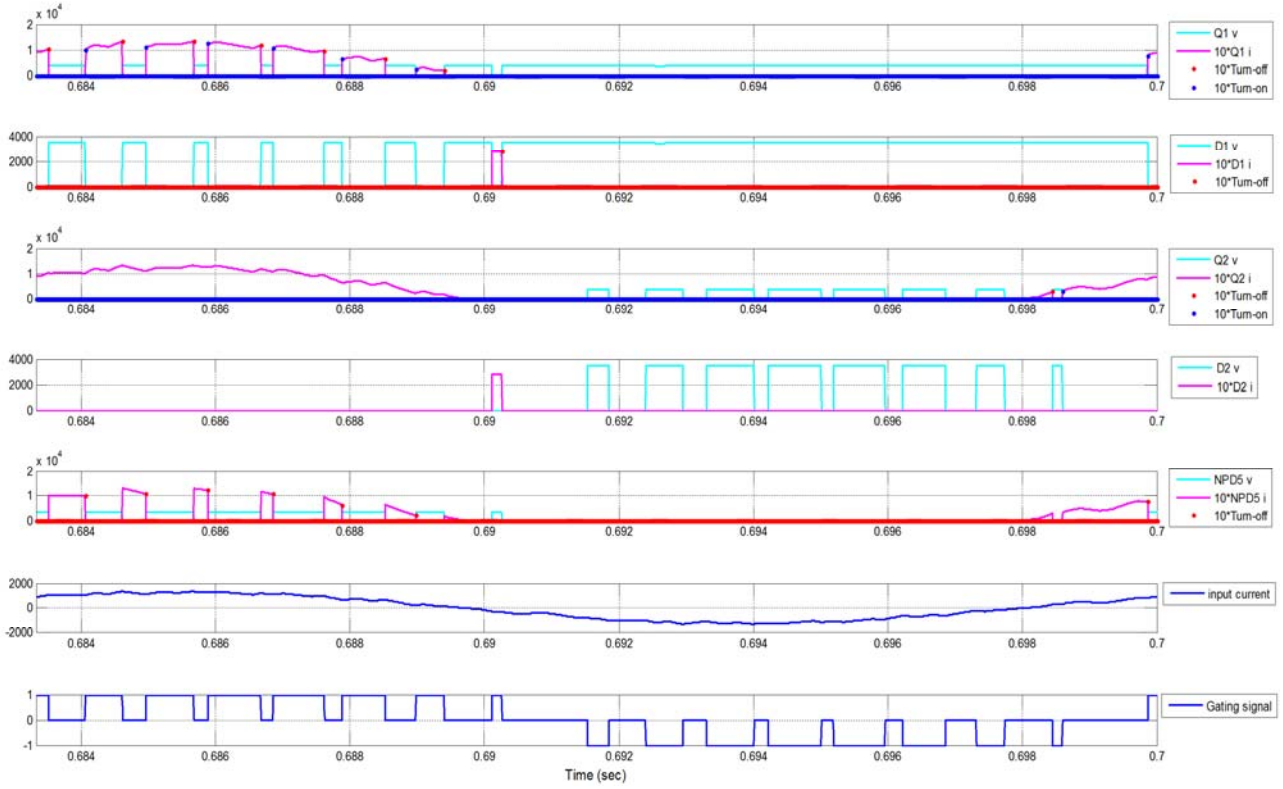


Fig. 9. Waveforms of switching voltage and current in the upper side of each phase-leg under inverter operating mode (*pf*=0.9 leading condition).

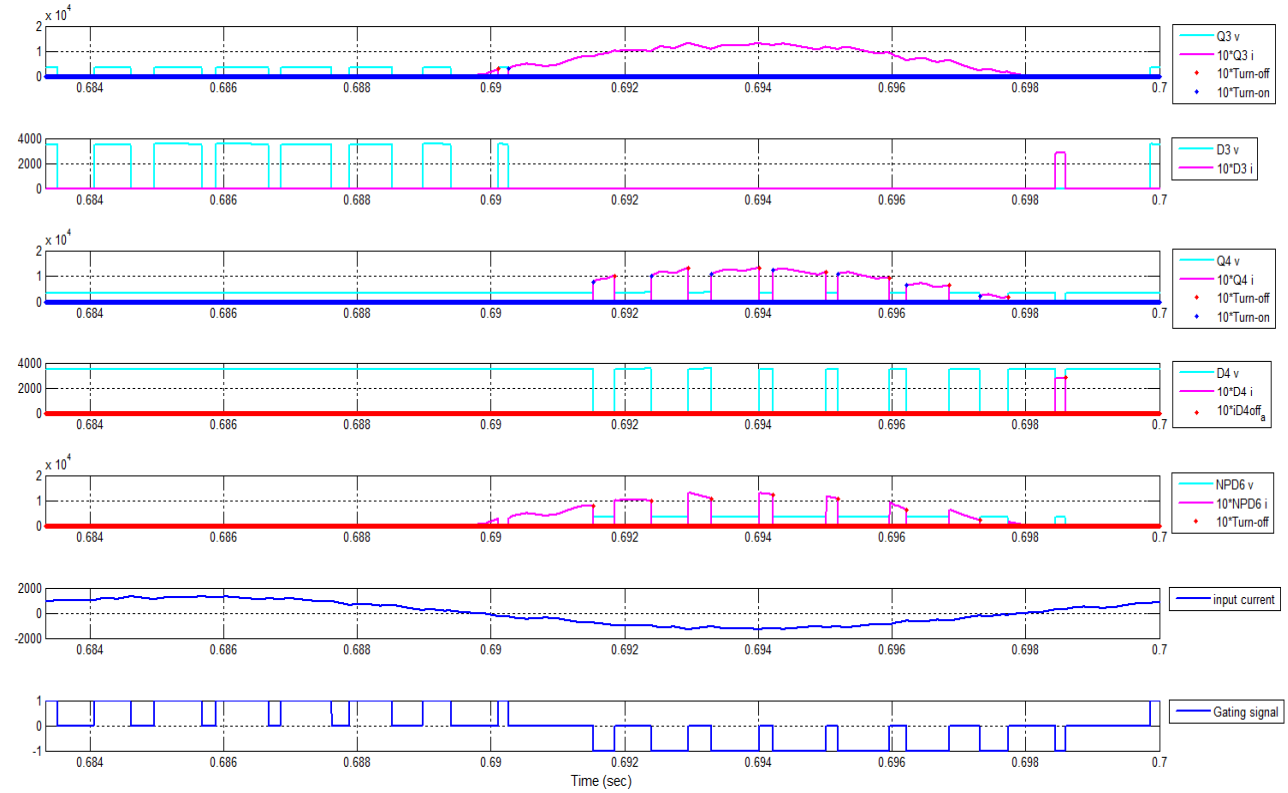


Fig. 10. Waveforms of switching voltage and current in the lower side of each phase-leg under inverter operating mode (*pf*=0.9 leading condition).

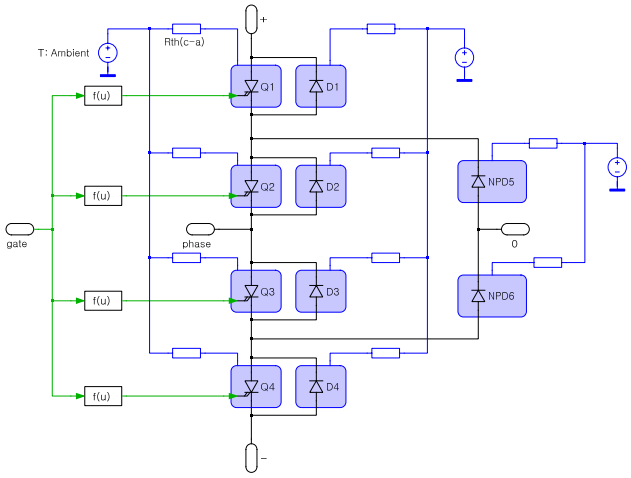


Fig. 11. Electrothermal model of each device for junction temperature in 3L-NPC VSC.

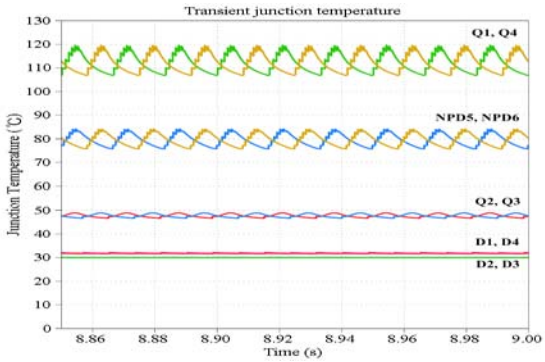


Fig. 12. Transient junction temperature of one phase-leg IGCT platform (*pf*=0.9 leading condition).

line period under the power factor of the 0.9 leading condition.

The converter operates under the inverter operating mode, i.e. power flows from the converter into the grid. In order to obtain the maximum semiconductor losses for the worst possible case, the simulation has been performed under the condition of a maximum ac input current; a line under-voltage of 90% and a power factor of the 0.9 leading condition. The switching voltage and current are sampled at the switching instant from the simulation waveform for each of the semiconductor devices. These sampled voltage and current values are then used to calculate the switching losses based on the specified loss values ($E_{on(spec)}$, $E_{off(spec)}$, and $E_{rr(spec)}$) given in the datasheet of the power semiconductors. The calculation of the switching loss is done in a linear manner as described in (4) - (6), assuming the typical gating impedances and snubber conditions suggested by the manufacturer.

### *C. Transient Junction Temperature*

The 3L-NPC VSC thermal model is built in PLECS to obtain the junction temperature profiles of the IGCT platform for each power device. Fig. 11 shows the main electrical and thermal circuit of the 3L-NPC VSC. Figs. 12-14 show the transient junction temperature of the one phase-leg IGCT

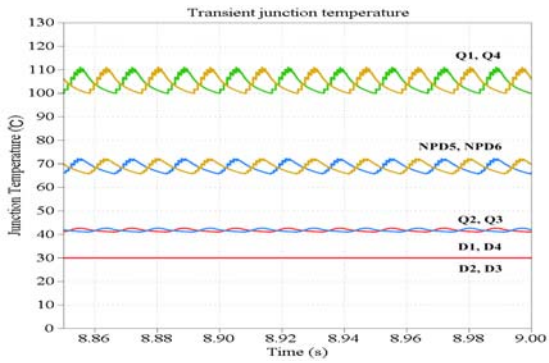


Fig. 13. Transient junction temperature of one phase-leg IGCT platform (*pf*=1.0 condition).

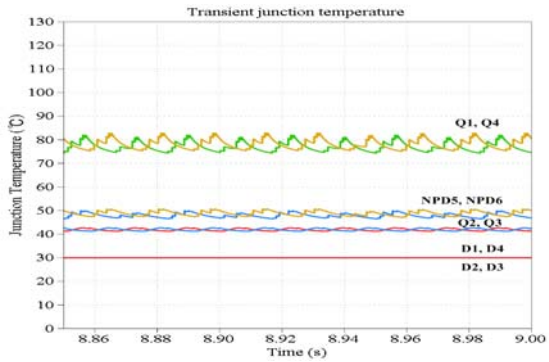


Fig. 14. Transient junction temperature of one phase-leg IGCT platform (*pf*=0.9 lagging condition).

platform under the three different power factor conditions (0.9 leading condition, 1.0, and 0.9 lagging condition) in a 5MW PMSG MV wind turbine.

In Fig 12, under the condition of a maximum ac input current, $Q_1$ and $Q_4$ are the most stressed device with a junction temperature of 120℃ and a temperature fluctuation of 13℃ amplitude. It can be seen that the mean temperature (111℃) of $Q_1$ and $Q_4$ is higher than the mean temperature (48℃) of $Q_2$ and $Q_3$. In addition, the mean temperature (32℃) of $D_1$ and $D_4$ is higher than the mean temperature (30℃) of $D_2$ and $D_3$ in the 3L-NPC VSCs. The mean temperatures (79℃) of $NPD_5$ and $NPD_6$ are similar to each other.

## V. COMPARISON OF LOSSES

The total power losses ($P_t$) of the semiconductor devices in a 5MW PMSG MV wind turbine are summarized in Fig. 15-17 using (1)-(6) under the 0.9 leading power factor condition of the inverter operating mode. The average conduction loss of each device is calculated by integrating the power loss of each device for one cycle of line frequency as shown in Fig. 8. The average conduction loss factor is calculated as in (2) and (3). The switching on and off loss factors are calculated based on the device voltage and current values sampled from the simulation waveform, as shown in Fig. 9 and Fig. 10. The total power loss ($P_t$) is then obtained by adding the

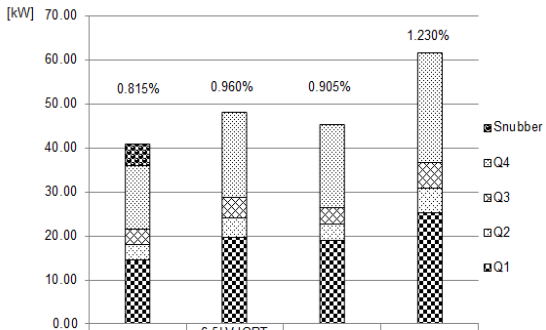


| | 6.5kV Press-pack IGCT | 6.5kV IGBT module (np=2) | 4.5kV Press-pack IGBT | 4.5kV Press-pack IEGT |
|---|---|---|---|---|
| Snubber | 4.92 | 0.00 | 0.00 | 0.00 |
| Q4 | 14.44 | 19.35 | 18.81 | 24.98 |
| Q3 | 3.41 | 4.58 | 3.74 | 5.69 |
| Q2 | 3.42 | 4.59 | 3.75 | 5.71 |
| Q1 | 14.54 | 19.47 | 18.93 | 25.13 |

Fig. 15. Total power loss ($P_t$) distribution in four devices ($Q_1$ - $Q_4$) of four different types of power semiconductors (Total power loss value for three-phase).

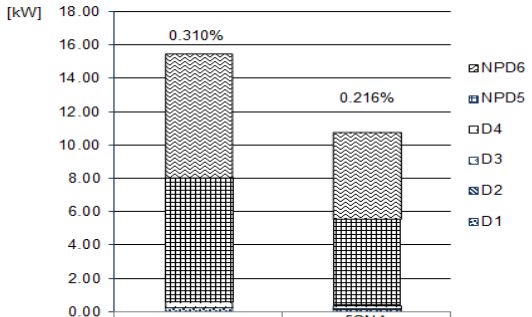


| | 5SDF10H6004 | 5SNA 0750G650300 (np=2) |
|---|---|---|
| NPD6 | 7.40 | 5.16 |
| NPD5 | 7.45 | 5.20 |
| D4 | 0.32 | 0.20 |
| D3 | 0.01 | 0.02 |
| D2 | 0.01 | 0.02 |
| D1 | 0.32 | 0.20 |

Fig. 16. Total power loss ($P_t$) distribution in six devices ($D_1$ - $D_4$, $NPD_5$ - $NPD_6$) of two different types of diodes; 5SDF10H6004, 5SNA0750G650300 (Total power loss value for three-phase).

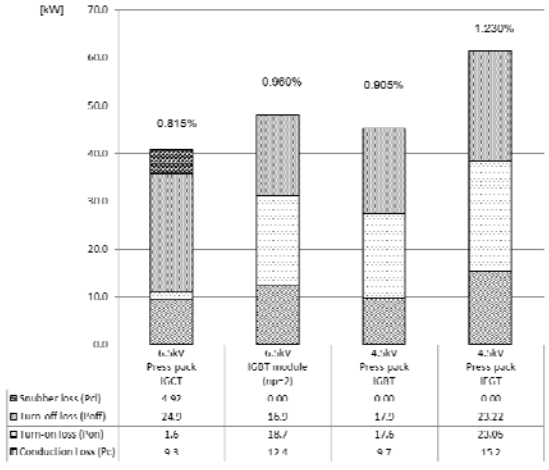


Fig. 17. Total power loss ($P_t$) distribution regarding conduction, switching, and snubber losses in four devices ($Q_1$ - $Q_4$) of four different types of power semiconductors (Total power loss value for three-phase).

conduction loss ($P_{cond}$) and switching loss ($P_{on}$ and $P_{off}$).

The total power losses of the four target semiconductor devices are compared including the snubber losses for the case of the IGCT. The power loss numbers in Fig. 15-17 represent the values for the complete 3-phase in a GSC of 5MW 3L-NPC VSCs as depicted in Fig. 7. In general, the turn-on losses of the anti-parallel diode and neutral-point clamp diode are very small, so they are ignored in this paper. For the case of a module type IGBT of 6.5kV/750A, it is necessary to employ two devices in parallel ($n_p$=2) to meet the converter operating specifications for an ac input current of 708A as shown in Table III. This parallel operation can be implemented either by paralleling devices or by paralleling two converter systems. In this paper, it is assumed that the current is shared equally between the two parallel devices of IGBT modules.

Figs. 15 and 16 show the total power loss ($P_t$) distribution in each device of the four different power semiconductors and the two different diodes using the power loss model (1)-(6) for the GSC of 3L-NPC VSCs. In Fig. 15-16, the switching devices show symmetrical power losses in one leg of the converter, i.e. the outer devices and the inner devices have almost same losses. The junction temperature of each switching device has been computed based on the thermal resistances given in Table I. The ambient temperature, i.e. the temperature of in-let cooling water, has been assumed to be 30 degrees. It is interesting to note that the inner anti-parallel diodes ($D_2$ and $D_3$) do not have switching off losses. This is due to the modulation characteristic of 3L-NPC VSCs, that is $Q_2$ and $Q_3$ being left turn on at the commutation instant of $D_2$ and $D_3$. In Fig. 16, a press-pack diode of 5SDF10H6004 is commonly employed as antiparallel and neutral-point clamp diode in the cases of press-pack type IGCTs, press-pack type IGBTs, and press-pack type IEGTs, for the sake of a fair comparison. In the case of module type IGBTs, the anti-parallel diode part integrated into the package of a 5SNA0750G650300 is also utilized as a neutral-point clamp diode. As for neutral-point clamp diodes of $NPD_5$ and $NPD_6$, two anti-parallel diodes of 5SNA0750G650300 are paralleled ($n_p$=2).

Fig. 17 provides the total loss ($P_t$) distribution regarding the conduction ($P_{cond}$), switching ($P_{on}$, $P_{off}$), and snubber losses ($P_{cl}$) in the four devices ($Q_1$, $Q_2$, $Q_3$, and $Q_4$) of four different types of power semiconductors using the power loss model (1) - (6). It is noted from the graph that the IGCT is subject to the largest switch turn-off loss among the four kinds of power devices. On the other hand, the IGCT has the smallest switch turn-on loss in the group. The total power loss dissipated in the snubber circuitry for the IGCT converter, as shown in Fig. 4, is shown to be around 4.92kW based on (8) and (9) for a three-phase GSC. Even with this additional power loss factor due to snubber circuitry, the switch turn-on loss of the IGCT is relatively smaller than those of the other power devices as shown in Fig. 17.

The total losses ($P_t$) of the 3L-NPC VSCs for 5MW PMSG

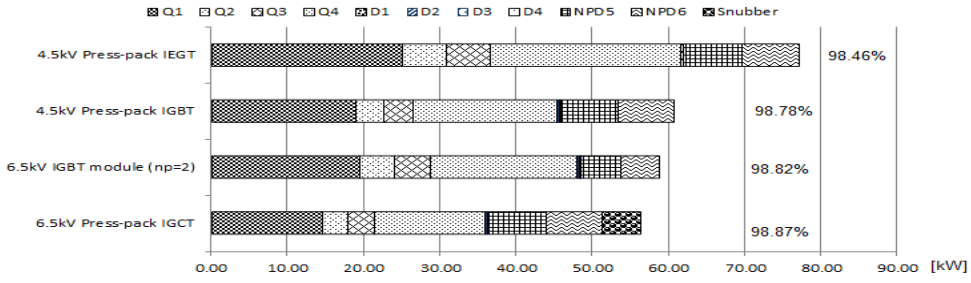


| | 6.5kV Press-pack IGCT | 6.5kV IGBT module (np=2) | 4.5kV Press-pack IGBT | 4.5kV Press-pack IEGT |
|---|---|---|---|---|
| Q1 | 14.54 | 19.47 | 18.93 | 25.13 |
| Q2 | 3.42 | 4.59 | 3.75 | 5.71 |
| Q3 | 3.41 | 4.58 | 3.74 | 5.69 |
| Q4 | 14.44 | 19.35 | 18.81 | 24.98 |
| D1 | 0.32 | 0.20 | 0.32 | 0.32 |
| D2 | 0.01 | 0.02 | 0.01 | 0.01 |
| D3 | 0.01 | 0.02 | 0.01 | 0.01 |
| D4 | 0.32 | 0.20 | 0.32 | 0.32 |
| NPD5 | 7.45 | 5.20 | 7.45 | 7.45 |
| NPD6 | 7.40 | 5.16 | 7.40 | 7.40 |
| Snubber | 4.92 | 0.00 | 0.00 | 0.00 |

Fig. 18. Total loss distribution regarding conduction, switching, and snubber circuit losses of four different types of power semiconductors (Total power loss value for three-phase at 1020Hz switching frequency).

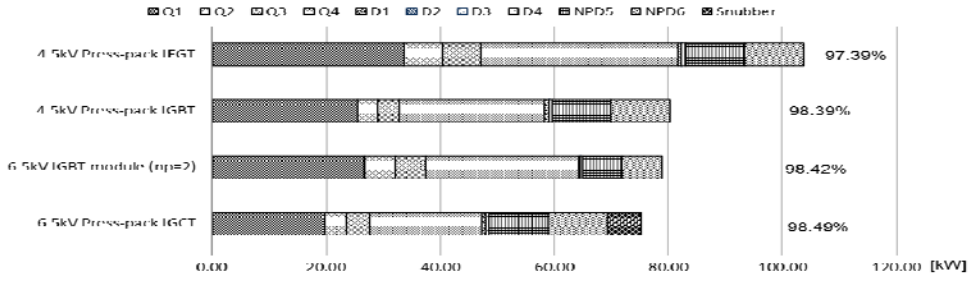


| | 6.5kV Press-pack IGCT | 6.5kV IGBT module (np=2) | 4.5kV Press-pack IGBT | 4.5kV Press-pack IEGT |
|---|---|---|---|---|
| Q1 | 19.65 | 26.68 | 25.50 | 33.66 |
| Q2 | 3.97 | 5.37 | 3.62 | 6.72 |
| Q3 | 3.96 | 5.37 | 3.61 | 6.72 |
| Q4 | 19.73 | 26.77 | 25.60 | 34.59 |
| D1 | 0.62 | 0.37 | 0.62 | 0.62 |
| D2 | 0.01 | 0.01 | 0.01 | 0.01 |
| D3 | 0.01 | 0.01 | 0.01 | 0.01 |
| D4 | 0.62 | 0.37 | 0.62 | 0.62 |
| NPD5 | 10.35 | 6.90 | 10.35 | 10.35 |
| NPD6 | 10.38 | 6.92 | 10.38 | 10.38 |
| Snubber | 6.00 | 0.00 | 0.00 | 0.00 |

Fig. 19. Total loss distribution regarding conduction, switching, and snubber circuit losses of four different types of power semiconductors (Total power loss value for three-phase at 1380Hz switching frequency).

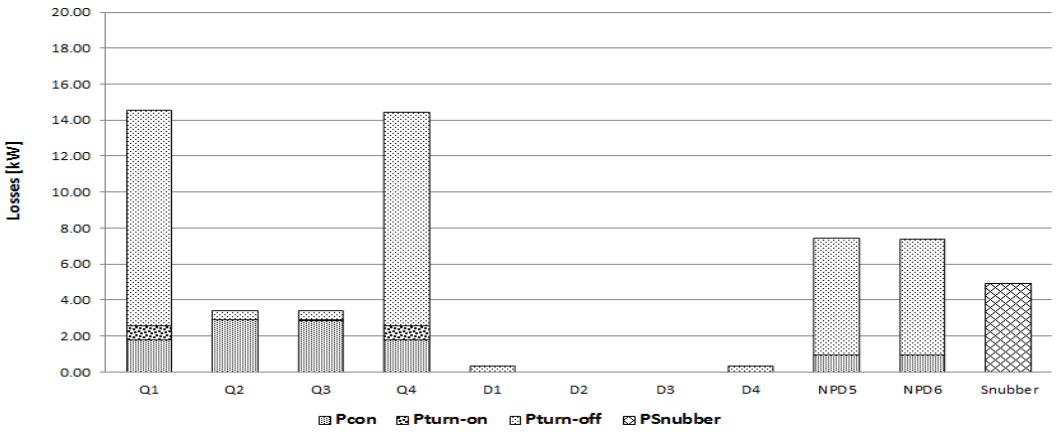


Fig. 20. Total loss distribution in semiconductor devices of three phase-leg under inverter operating mode employing 6.5kV IGCT (*pf*=0.9 leading condition).

MV wind turbines are described in Fig. 18 for each device in a one phase-leg IGCT platform (*pf*=0.9 leading condition) using the power loss model (1)-(6). It shows that the press-pack type IGCT has the lowest loss value, 56kW (1.13%), among all four kinds of power semiconductor platforms including the snubber losses. On the other hand, the press-pack type IEGT has the highest loss value at 77kW (1.54%). The module type IGBT exhibits a loss value of 58kW (1.18%) which is close to that of the press-pack type IGCT. The press-pack type IGBT has a loss value of 61kW (1.22%). The power loss of the module type IGBT corresponds to the case of two devices in parallel ($n_p$=2). In this paralleling of devices or converters, the equal sharing of current becomes an important design task. However, it may further complicate the control algorithm or mechanical concept when compared to single device approaches such as the IGCT, press-pack IGBT, and press-pack IEGT.

In order to investigate the influence of switching frequency on the loss characteristic, a loss analysis for a switching frequency of 1380Hz has been performed. It is noted from Fig. 19 that the loss has been increased by approximately 0.4% for the cases of the press-pack IGBT, module IGBT, and IGCT. It is interesting to note that the press-pack IEGT has the largest increase of loss by approximately 1.0%.

Fig. 20 describes the total loss distribution at worst possible case under the inverter operating mode for the target power semiconductor switch of the IGCT type. Under the inverter operating mode, $Q_1$, $Q_4$, $NPD_5$, and $NPD_6$ are subject to most of the power loss. As noted in Fig. 8, the amplitude of the ac input current at the converter pole changes as the power factor is varied from 0.9 leading to 0.9 lagging under the rated output power generation. A higher amplitude of the ac input current at the converter pole naturally results in higher power losses in the power semiconductor switches. In addition, a different power factor angle also changes the loss distribution pattern among the power semiconductor devices in each phase leg due to the commutation property in 3L-NPC VSCs.

## VI. CONCLUSION

In this paper, the loss analysis of a 6.5kV/3800A press-pack type IGCT, 4.5kV/2400A press-pack type IGBT, 4.5kV/2100A press-pack type IEGT, and 6.5kV/750A module type IGBT for 5MW PMSG MV wind turbines employing a back-to-back type 3L-NPC VSC is presented. The transient thermal junction temperature of the IGCT platform is described in GSC for 5MW PMSG MV wind turbines. The switching loss is obtained under the assumption of typical gate impedance and snubber conditions provided by the semiconductor manufacturers. The switching frequency is set to 1020Hz, under a grid side input voltage of 4.16kV. The press-pack type IGCT has been found to have the lowest device losses, i.e. the highest efficiency, among the four candidates with the additional snubber loss of the IGCT being taken into consideration. The module type IGBT requires that two devices be put in parallel in order to meet the given operating specifications of an ac input current of 708A. This paralleled devices structure may complicate the mechanical and cooling systems which are very critical functional elements in multi-MW WTSs. Considering the difficulty of measuring the losses of high power converters in the MW range in the lab, the method of loss analysis proposed in this paper has practical usefulness since it can accurately estimate the losses of the high power semiconductor devices in 5MW PMSG MV wind turbines based on the semiconductor device datasheets. An experimental verification of these comparison results is in progress and the results will be reported in future publications.

## ACKNOWLEDGMENT

This work was supported by the National Research Foundation of Korea (NRF) grant funded by the Korea government (MSIP) (No. 2010-0028509) & (No. 2014R1A2A1A11053678).

## REFERENCES

[1] World Market Update 2008 (Forecast 2009-2013), BTM Consult ApS, Ringøkbing Denmark, Mar. 2009.

[2] S. Kouro, M. Malinowski, K. Gopakumar, J. Pou, L. G. Franquelo, B.Wu, J. Rodriguez, M. A. Perez, and J. I. Leon, "Recent advances and industrial applications of multilevel converters," *IEEE Trans. Ind. Electron.*, Vol. 57, No. 8, pp. 2553-2580, Aug. 2010.

[3] J. Rodriguez, S. Bernet, P. K. Steimer, and I. E. Lizama, "A survey on neutral-point-clamped inverters," *IEEE Trans. Ind. Electron.*, Vol. 57, No. 7, pp. 2219-2230, Jul. 2010.

[4] O. Senturk, L. Helle, S. Munk-Nielsen, P. Rodriguez, and R. Teodorescu, "Power capability investigation based on electro-thermal models of press-pack IGBT three-level NPC and ANPC VSCs for multi-MW wind turbines," *IEEE Trans. Power Electron.*, Vol. 27, No. 7, pp. 3195-3206, 2012.

[5] Y. S. Suh, J. Steinke, and P. Steimer, "Efficiency comparison of voltage source and current source drive system for medium voltage applications," *IEEE Trans. Ind. Electron.*, Vol. 54, No. 5, pp. 2521-2531, Oct. 2007.

[6] A. Faulstich, J. K. Steinke, and F. Wittwer, "Medium voltage converter for permanent magnet generators up to 5MW," in *Proc. Eur. Conf. Power Electron. Appl.*, pp. 1-9, 2005.

[7] A. Zuckerberger, E. Suter, C. Schaub, A. Klett, and P. Steimer, "Design, simulation and realization of high power NPC converters equipped with IGCTs," in *Proc. of the Thirty-Third IAS Annual Meeting*, Vol. 2, pp.865-872, 1998.

[8] J. Rodriguez, S. Bernet, B. Wu, J. Pontt, and S. Kouro, "Multilevel voltage-source-converter topologies for industrial medium-voltage drives," *IEEE Trans. Ind. Electron.*, Vol. 54, No. 6, pp. 2930-2945, Dec. 2007.

[9] S. Bernet, "Recent developments of high power converters for industry and traction applications," *IEEE Trans. Power Electron.*, Vol. 15, No. 6, pp. 1102-1117, Nov. 2000.

[10] S. Bernet, E. Carroll, P. Streit, O. Apeldoorn, P. Steimer, and S. Tschirley, "10 kV IGCTs," *Industry Application*

*Magazine*, Vol. 11, No. 2, pp. 53-61, Mar./Apr. 2005.
[11] "Asymmetric Integrated Gate-Commutated Thyristor 5SHY 42L6500", Datasheet, Doc. No. 5SYA1245-03 Dec. 12, ABB Switzerland Ltd., Online: www.abb.com.
[12] "Fast Recovery Diode 5SDF 10H6004", Datasheet, Doc. No. 5SYA1109-03 January. 10, ABB Switzerland Ltd., Online: www.abb.com.
[13] "IGBT Moduled 5SNA 0750G650300", Datasheet, Doc. No. 5SYA 1600-02 04-2012, ABB Switzerland Ltd., Online: www.abb.com.
[14] Alvarez, R. Filsecker, and S. Bernet, "Characterization of a new 4.5 kV press pack SPT+ IGBT for medium voltage converters," in *Proc. of the 1st IEEE Energy Conversion Congress and Exposition, ECCE 2009,* pp. 3954-3962, 2009.
[15] "Insulated Gate Bi-Polar Transistor, Type T2400GB45E", Datasheet, T2400GB45E Nov. 2011, IXYS, Online: www.westcode.com.
[16] Kon, K. Nakayama, S. Yanagisawa, J. Miwa, and Y. Uetake, "The 4500V-750A planar gate press pack IEGT," in *Proc. ISPSD'98*, pp. 81-84, 1988.
[17] K. Ichikawa, M. Tsukakoshi, and R. Nakajima, "Higher efficiency three-level inverter employing IEGTs," in *Proc. 19th Annu. IEEE APEC*, Vol. 3, pp. 1663-1668, 2004.
[18] "Toshiba Silicon N-Channel IEGT ST1200GXH24A", Datasheet, 2009-09-07, Toshiba Ltd, Online: www.semicon.toshiba.co.jp.
[19] P. Alemi and D. C. Lee, "Comparative analysis of power losses for three-level T-type and NPC PWM inverters," *Transactions of Korean Institute of Power Electronics(KIPE)*, Vol. 19, No. 2, pp. 173-183, Apr. 2014.
[20] M. K. Kim, D. G. Woo, B. K. Lee, N. J. Kim, and J. S. Kim, "Loss analysis of power conversion equipment for efficiency improvement," *Transactions of Korean Institute of Power Electronics(KIPE)*, Vol. 19, No. 1, pp. 80-90, Feb. 2014
[21] L. Clotea and A. Forcos, "Power losses evaluation of two and three-level NPC inverters considering drive applications," in *Proc. OPTIM,* pp. 929-934, 2012.
[22] M. Buschendorf, J. Weber, and S. Bernet, "Comparison of IGCT and IGBT for the use in the modular multilevel converter for HVDC applications," in *Proc. 9th Int. Multi-Conf. SSD*, pp. 1-6, 2012.
[23] D. Zhou, F. Balabjerg, M. Lau, and M. Tonnes, "Thermal cycling overview of multi-megawatt two-level wind power converter at full grid code operation," *IEEJ Trans. Ind. Appl.*, Vol. 2, No. 4, pp. 173-182, 2013.
[24] K. Ma and F. Blaabjerg, "Thermal optimized modulation methods of three-level neutral-point-clamped inverter for 10MW MW wind turbines under low-voltage ride through," *IET Power Electron.*, Vol. 5, No. 6, pp. 920-927, Jul. 2012.
[25] C. Sintamarean, F. Blaabjerg, and H. Wang, "A novel electro-thermal model for wide bandgap WBG-semiconductor based devices," *IEEE European Conference on Power Electronics and Applications*, EPE - ECCE Europe, 2013.
[26] ABB Application Note: 'Applying IGBTs', May 2007.
[27] H. Wang, A. M. Khambadkone, and X. Yu, "Control of parallel connected power converters for low voltage microgrid – Part II: Dynamic electrothermal modeling," *IEEE Trans. Power Electron.*, Vol. 25, No. 12, pp. 2971-2980, Dec. 2010.
[28] A. Rockhill, M. Liserre, R. Teodorescu, and P. Rodriguez, "Grid-filter design for a multi megawatt medium-voltage voltage-source inverter," *IEEE Trans. Ind. Electron.*, Vol. 58, No. 4, pp. 1205-1217, 2011.

**Kihyun Lee** was born in the Republic of Korea, in 1982. He received his B.S. degree in Electronic Engineering from Chonbuk National University, Jeonju, Korea, in 2008, where he is presently working towards his M.S. degree in Electrical Engineering. From 2008 to 2012, he was a Research Engineer in the High Power Discrete Division of KODENSHI AUK Co., Korea. His current research interests include high power conversion systems for renewable energy sources and medium electric drive systems.

**Yongsug Suh** (M'90/SM'07) was born in Seoul, Korea. He received his B.S. and M.S. degrees from Yonsei University, Seoul, Korea, in 1991 and 1993, respectively, and his Ph.D. degree in Electrical Engineering from the University of Wisconsin, Madison, WI, USA, in 2004. From 1993 to 1998, he was an Application Engineer in the Power Semiconductor Division of Samsung Electronics Co., Korea. From 2004 to 2008, he was a Senior Engineer in the Power Electronics & Medium Voltage Drives Division of ABB, Turgi, Switzerland. Since 2008, he has been with the Department of Electrical Engineering, Chonbuk National University, Jeonju, Korea, where he is currently an Associate Professor. His current research interests include power conversion systems of high power for renewable energy sources and medium voltage electric drive systems.

**Yongcheol Kang** received his B.S., M.S., and Ph.D. degrees from Seoul National University, Korea, in 1991, 1993, and 1997, respectively. He has been with Chonbuk National University, Jeonju, Korea, since 1999. He is currently a Professor at the Department of Electrical Engineering, Chonbuk National University, and the director of the WeGAT Research Center supported the Ministry of Science, ICT, and Future Planning (MSIP), Korea. His current research interests include the development of new protection and control systems for wind power plants and wind energy integration technologies.